

A model of the ULF magnetic and electric field generated from a dust devil

W. M. Farrell,¹ J. R. Marshall,² S. A. Cummer,³ G. T. Delory,⁴ and M. D. Desch¹

Received 31 January 2006; revised 25 May 2006; accepted 6 July 2006; published 17 November 2006.

[1] It has been demonstrated that terrestrial dust devils emit ULF magnetic radiation. On Mars, dust devils may also generate such magnetic emissions, which might be used as a hazard alert for manned missions. Specifically, grains in dust devils become charged via contact electrification, and it has been proposed that the cyclonic motion of these charged grains in the vortex wind fields accounts for the magnetic emission. To test this hypothesis in general and the possible Mars application, a computer simulation of the contact electrification/wind blowing phenomena was created, with the charge distribution and resulting magnetic fields monitored as a function of time. The results indicate that indeed a fluctuating charge distribution in a vortex wind can account for the ULF magnetic fields measured from a dust devil. The contact electrification process is a function of composition, and we demonstrate that the various compositions will give rise to different magnetic field responses from the dust devil. We also demonstrate that this system of swirling charged grains develops vertical currents and associated electric fields, as suggested in preceding works.

Citation: Farrell, W. M., J. R. Marshall, S. A. Cummer, G. T. Delory, and M. D. Desch (2006), A model of the ULF magnetic and electric field generated from a dust devil, *J. Geophys. Res.*, *111*, E11004, doi:10.1029/2006JE002689.

1. Introduction

[2] Given the new NASA emphasis on exploration of Mars, there is renewed interest in Martian meteorological phenomena that could adversely impact human and robotic presence on the surface. Dust devils and dust storms, in particular, have the potential to be at least a nuisance by obscuring vision and layering sensitive surfaces (such as solar power panels), to possibly being a bonafide hazard via their electrical effects and the potential grain toxicity [Beatty *et al.*, 2005]. Laboratory [Eden and Vonnegut, 1973; Mills, 1977] and terrestrial field tests [Freier, 1960; Crozier, 1964; Delory *et al.*, 2002; Farrell *et al.*, 2004; Jackson and Farrell, 2006] indicate that dust devils are highly charged via contact electrification in regions where grain-grain collisions are large. Vertical winds in dust devil tend to mass stratify grains, which by nature, also separates grains by charge polarity, thereby creating an interstorm macroscopic electric dipole moment on the order of 0.5 C-m [Crozier, 1964; Jackson and Farrell, 2006]. While vertical dust devil winds create a large electrostatic field, vortex-like winds swirl the charged grains in quasi-cyclonic motion. Such motion has been suggested to give rise to a magnetic

emission. This emission was recently detected from terrestrial dust devils [Houser *et al.*, 2003; Farrell *et al.*, 2004]. In this paper, we will present a computer model of the contact electrification and vortex-wind process, and demonstrate the viability of such winds to create the magnetic field emissions.

[3] The original detection of ULF magnetic emissions from dust devils occurred in Eldorado Valley near Boulder City, NV, in July of 2000 [Houser *et al.*, 2003]. A magnetic search coil antenna sensitive between 1 Hz and 20 kHz was mounted to a forward-extending boom of a truck, and the truck pursued dust devils on the several square kilometer dried lake bed. One very large fully matured dust devil was intercepted and ULF magnetic noise was detected that persisted for over 30 seconds as the aeolian structure receded from the truck. Figure 1 shows the emission during the passage of the feature.

[4] The ULF magnetic emission was detected at frequencies below 50 Hz, with peak emissions near 10 Hz [Houser *et al.*, 2003]. The emission intensity remained nearly flat for the first 15 s after interception, but then reduced in intensity approximately as $B \sim r^{-2.4}$ for the next 20 s as the dust devil traversed beyond ~ 50 -m from the truck. Houser *et al.* [2003] suggested that this ULF magnetic emission is the result of the cyclonic motion of the charge grains in the dust devil behaving as a current loop or solenoid. A time-stationary solenoid would produce a DC magnetic field. However, the dust devil is a fluctuating, undulating solenoid, with ever-changing horizontal cross-sectional area and with temporally varying dust density inhomogeneities. These temporal variations can possibly give rise to a fluctuating magnetic field (AC magnetic field).

¹NASA Goddard Space Flight Center, Greenbelt, Maryland, USA.

²SETI Institute, Mountain View, California, USA.

³Department of Electrical and Computer Engineering, Duke University, Durham, North Carolina, USA.

⁴Space Sciences Laboratory, University of California, Berkeley, Berkeley, California, USA.

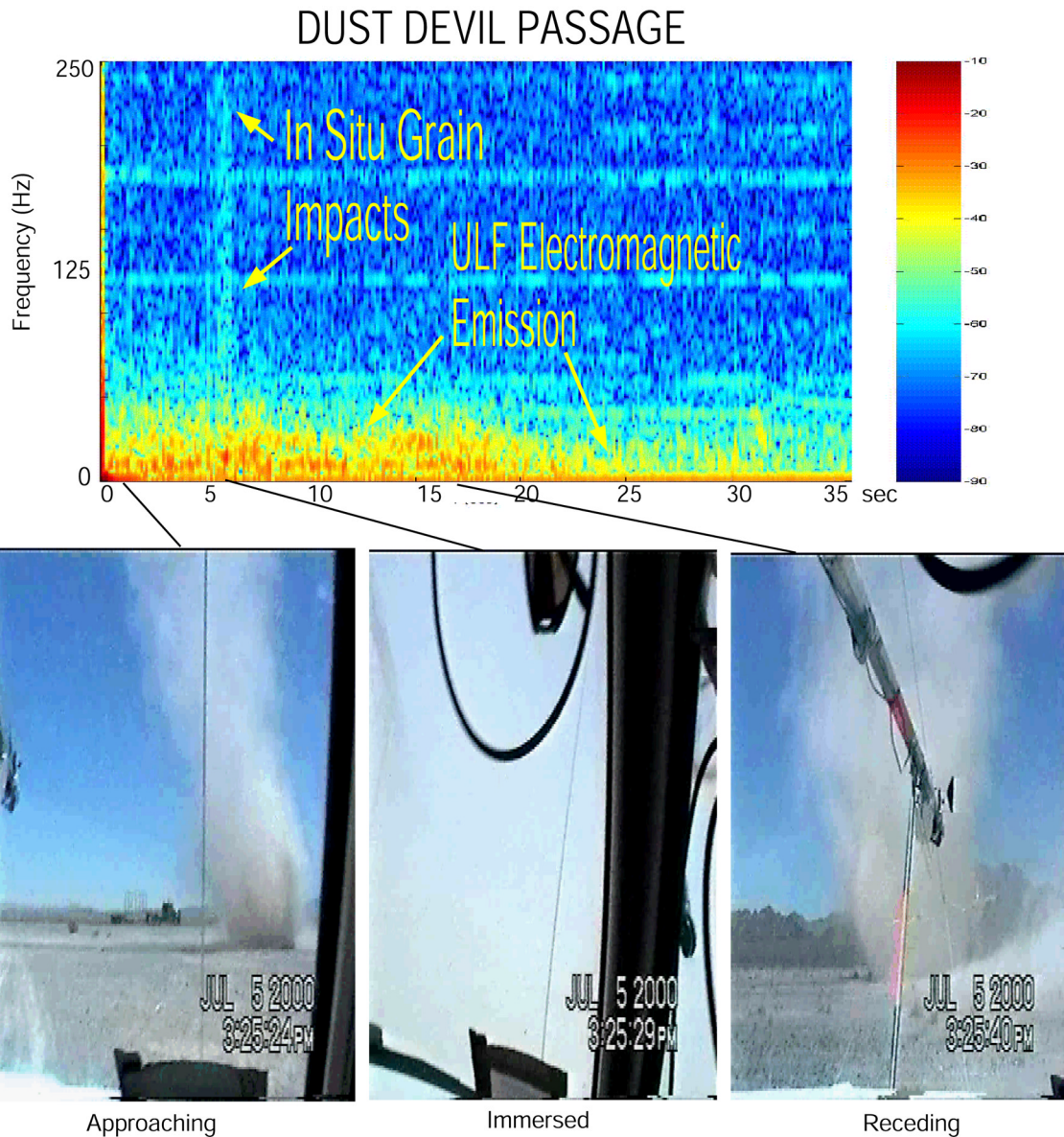


Figure 1. The ULF magnetic emissions detected from a truck-intercepted dust devil. The in situ grain-antenna impacts occurred when fully immersed in the dust devil, and are associated with grain charge transfer to exposed capacitive elements of the antenna. A second ULF emission was detected that became weaker as the feature receded from the truck. The truck was stationary for the interception and subsequent recession period. See *Houser et al.* [2003] for more details regarding this event.

[5] A second dust devil detected in the Arizona desert during a 2002 field test also produced ULF magnetic emission [Farrell *et al.*, 2004]. In this case, the emission was between 1 and 10 Hz and was found at power levels nearly a factor of 1000 times greater than background levels. The emission was not broadbanded but possessed a distinct emission peak at a 3 Hz and half-power bandwidth of about 1 kHz ($Q \sim 3$) suggesting a surprisingly narrow-banded emission. Assuming a solenoid dust devil generator, the currents responsible for the magnetic field were found to be consistent with a charge density of $\sim 10^6$ e/cc for winds speeds in the tens of meters per second. The ULF magnetic energy in the dust devil was found to be about one part in 100 million of the electrostatic energy, suggesting that

magnetic emission, while detectable, is a small fraction of the overall energy in the grain charging/charge stratification process [Farrell *et al.*, 2003, 2004].

[6] Prior modeling [Melnik and Parrot, 1998] and analog studies suggests that Martian dust devils behave in a very similar way to their terrestrial counterparts. They are driven by a similar atmospheric instability process, contain cyclonic winds, and warmed cores [Ryan and Lucich, 1983]. Lifted Martian dust grains are also expected to be electrically-charged and thus should also emit magnetic fields via the same processes described for the terrestrial case. Such ULF magnetic emission might act as a hazard alert for explorers to possible incoming dust devils and larger storms.

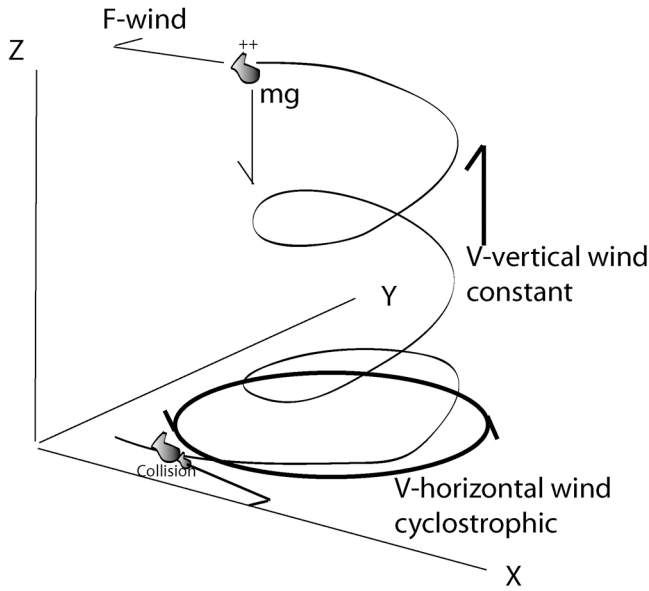


Figure 2. An illustration of the model showing the cyclostrophic winds in the X/Y plane and vertical winds along z.

[7] In order to better understand the physical processes, including grain charging, cyclonic motion, and ULF emission, occurring generally in dust devils and for applications on Mars we now model the charging cyclonic grain motion using a three-dimensional particle code. The objective of the simulation is to determine if initially uncharged, stationary grains can be mixed and moved in cyclonic motion to give rise to the magnetic emissions. We run the simulations for a Martian atmosphere to understand the effect on that planet and its possibility as a hazard alert. The next section describes the tribocharging model applied while the section thereafter presents the modeling results.

2. Model Description

[8] In order to quantify the magnetic fields generated from a set of swirling charges, a numerical model was developed that featured the movement of simulated grain charges in dust devil-like cyclostrophically balanced wind pattern. This model is called the microscopic triboelectric simulator (MTS) and incorporates particle movement and charge exchange upon grain-grain contact. An illustration of the model is shown in Figure 2. The x and y axis represent horizontal dimensions while the z axis is oriented in the vertical direction. The force of gravity is acting along the $-z$ direction.

[9] The prevailing winds in the horizontal plane are defined by a pattern in cyclostrophic balance where the outward centripetal force of a given fluid element is balanced against the dust devil pressure gradient drawing the fluid element radially inward. The balance of these forces creates circular fluid element trajectories about the dust devil center. This balance is discussed by *Greeley et al.* [2003], and the equation of motion for the gas fluid element is

$$\rho_a v_h^2 / r = \partial P / \partial r, \quad (1)$$

where ρ_a is the atmospheric density (for Mars), v_h is the fluid tangential (horizontal) velocity, and r is the distance from the dust devil center. *Greeley et al.* [2003] ran a series of lab experiments for general meteorological properties for dust devils at Earth and Mars. As suggested by the composite dust devil pressure profile provided in their Figure 5, the typical system pressure is “well-shaped” having a local minimum in the central region ($r = 0$), defined here as P_m , and appears to exponentially rise to ambient levels, P_a with increasing distance from the center. As such, one can analytically express this pressure well via

$$P(r) = P_a(1 - \Delta P \exp(-kr)/P_a), \quad (2)$$

where $\Delta P = P_a - P_m$, k is the inverse of the scale size of the dust devil, and r is the horizontal distance (radial magnitude in cylindrical coordinates) from the dust devil center. Given this pressure, the velocity can be expressed via equation (1) as

$$\mathbf{v}_h = -A \exp(-kr)(y - y_0)/r^{1/2} \mathbf{x} + A \exp(-kr)(x - x_0)/r^{1/2} \mathbf{y}, \quad (3)$$

where $A = (k\Delta P/\rho_a)^{1/2}$ and \mathbf{x} and \mathbf{y} are unit vectors. Upward vertical winds of constant velocity can also be included in the simulation (but are not dynamically coupled to the horizontal winds). Such vertical winds result from surface heating and have been analytically defined by *Rennó and Ingersoll* [1996] and *Rennó et al.* [1998].

[10] A set of grains are placed at a location in the box in close proximity to each other, with an initial velocity of zero. The individual grain radius is defined as

$$a = a_0 / (0.005 + \text{RANDOM}(0, 1)), \quad (4)$$

where $\text{RANDOM}(0,1)$ is a random number between 0 and 1 and $a_0 = 0.05 \mu\text{m}$. Note that this form of the distribution yields the smallest value of grain radius of $0.05 \mu\text{m}$, largest value at $10 \mu\text{m}$, and median value near $0.1 \mu\text{m}$. This form guarantees that there will be many more smaller grains in the simulation. For example, in each sample of 100 grains and an assumed truly random number generation process, the set will likely contain only one grain with radius exceeding $3.3 \mu\text{m}$ ($a_0/0.015$), but nearly 50 grains with radius below $0.1 \mu\text{m}$ ($a_0/0.505$).

[11] The composition of the grains is also allowed to vary and we impose a compositional mix to maximize the triboelectric surface potential difference between larger and smaller grains. Specifically, we apply the grain/grain contact electrification algorithm presented by *Desch and Cuzzi* [2000]. Their equations (5)–(10) describe the triboelectric charge transfer following a collision, with new (post-collision) grain charge q_1' and q_2' on grain 1 and 2, respectively, being

$$\begin{aligned} q_1' &= a_1 q_{\text{tot}} + a_2 \Delta\Phi \\ q_2' &= a_3 q_{\text{tot}} + a_4 \Delta\Phi, \end{aligned} \quad (5)$$

where q_{tot} is the total precollision charge on both grains ($q_1 + q_2$) and $\Delta\Phi$ is the difference in surface contact

(triboelectric) potential (which is large for grains of vastly different conductivities like insulators and metals [see *Desch and Cuzzi*, 2000, Table 2]). The quantities a_1 – a_4 are functions of the grain–grain mutual capacitances defined by *Desch and Cuzzi* [2000]. If grains are of similar composition such that $\Delta\Phi = 0$, charge is still exchanged owing to the differing grain sizes (differing grain capacitances). However, if $\Delta\Phi$ is not zero, the relative composition of the grains becomes an important factor. For a mixture of insulators and metals (where $\Delta\Phi \sim 2$ V), charge exchange via compositional effects greatly exceed the process based on relative size (capacitance). A comparison of the two triboelectric processes (size-only versus composition) was presented by *Farrell et al.* [2003].

[12] As described by *Desch and Cuzzi* [2000], if the grain distribution consists of all silicates (insulators), then little charge is exchanged between the many small and few large grains because the triboelectric process is not overly efficient for grains of similar composition. If however, fine conductive (metallic) grains are added, then each conductive grain collision with a larger silicate grain will result in the transfer of many thousands of electrons to the light metallic grain (leaving the heavy silicate with a net positive charge). Within a dust devil, as vertical winds blow, the light negative grain then moves upward forming the inverted electric dipole moment like those reported by *Freier* [1960], *Crozier* [1964], *Delory et al.* [2002], and *Jackson and Farrell* [2006]. To mimic this behavior in our simulation, we vary the grain composition in such a way that there are many fine conductive grains with radius $< 2 \mu\text{m}$ and a fewer large insulating grains with $r \gg 2 \mu\text{m}$. The triboelectric potential difference, $\Delta\Phi$, between these grains is initially set at ~ 1.6 V consistent with Table 2 of *Desch and Cuzzi* [2000]. The small conductive grains will then charge negative in our simulation and become spatially displaced relative to the large heavy positive insulator grains (see Results section). We also present simulation results where $\Delta\Phi$ is both vastly reduced (to appear more like that “silicate-only” case) and vastly increased (unrealistically) to determine the effect of grain composition on resulting emission.

[13] We assume grains of mixed composition, but is there a scenario to explain the presence of large insulator/small metallic grains. One possibility explanation similar to that presented by *Greeley et al.* [1992] is that larger silicate grains contain smaller, embedded metallic grains. For example, a sand formed from eroded granite would consist primarily of silicates, but also would have a small percentage of alumina and iron. Upon collisions with each other and the surface, the large insulator grains erode, releasing the smaller metallic grains (and a finer silicate powder). The large insulator grains remain in saltation while the smaller metallic grains are easily transported upward via the vertical winds. *Cahill et al.* [2005] reported that the sand/dust at White Sands NM contain basalt-like grains with a population of smaller metallic grains. Such a mixed composition would be very tribo-electrically active. On Mars, an even more tribopotentially diverse grain assortment is expected, leading to charged grains.

[14] We note that the grain–grain charge exchange process defined by *Desch and Cuzzi* [2000] is microscopic in nature, but we also monitor charge grain movement at mesoscale sizes (meters) which places computational limits on the

simulation. We discuss this issue below. Also, we recognize that *Desch and Cuzzi*’s algorithm is self-consistent but may not include all aspects of grain charging. Hence more complicated algorithms can be applied in the code but for this work, we limit the charge exchange process to that defined by *Desch and Cuzzi* [2000].

[15] The primary simulated forces acting on the grains are gravity and wind forces defined as

$$\mathbf{F}_w = \pi r^2 \rho_a (\mathbf{v} - \mathbf{v}_g)^2 \underline{\mathbf{v}}', \quad (6)$$

where ρ_a is the Martian atmospheric density ($1.6 \times 10^{-2} \text{ kg/m}^3$), \mathbf{v} is the wind field velocity, \mathbf{v}_g is the grain speed, and \mathbf{v}' is the difference between the two, $\mathbf{v}' = \mathbf{v} - \mathbf{v}_g$. The variable \mathbf{v}' is the \mathbf{v}' unit vector. The grains are charged and electric forces are present in the dust cloud. However, such forces are anticipated to be small in comparison to driving meteorological forces on the grains. In our model, fluid forces are assumed to move the grains (these terms are kept in the equation of motion) and we assume electromagnetic forces on the grains are not significant in grain dynamics.

[16] The initially uncharged grains are located at specific locations in the simulation box, and prevailing winds move the grains. Some fraction of the grains collide and generate/exchange charge based on equation (5) and the dynamics of the charge grains under the prevailing influences of winds and gravity is calculated. We do not attempt to model the detailed lifting process from the surface, which involves a combination of the dust devil pressure gradient and wind shear stress to offset the force of gravity and surface cohesion [*Greeley et al.*, 2003]. Instead, we assume that the grains are already away from the surface and are then influenced only by winds and gravitational forces in the low-pressure dust devil. In essence, we model a case where the grains are suspended at $t = 0$, but then feel the full and direct force of the winds and gravity thereafter. Note that our objective is to understand grain contact electrification and subsequent grain charge separation in the cyclonic winds that may lead to the development of magnetic fields. Hence the details of near-surface dynamics is not as critical in our analysis as the actual charged grain separation process in the winds themselves, the latter of which is modeled herein.

[17] When possible, the units of the model are scaled to MKS. As such, each time step is approximately 1 ms and the simulation is run for ~ 0.5 s (500 time steps). The simulation box is $2 \text{ m} \times 2 \text{ m} \times 1 \text{ m}$ with a spatial resolution in each dimension of 1 cm. Each grain radius and mass is kept in MKS units. The quantity A and k in equation (3) are $56 \text{ m}^{1/2}/\text{s}$ and 10 m^{-1} , respectively. Because of the complexity of the code and the run time, a limited number of grains are simulated (~ 1200). To correlate dust quantity to a true dust devil, we are required to multiply the grain density in our simulation to that of a real dust devil. In order to determine the magnetic field from the grains, we calculate the vector magnetic potential, \mathbf{A} , treating each grain as an independent current source with current directly proportional to grain charge, q , and velocity, \mathbf{v}_g . A relative magnetic field is then derived via $\mathbf{B}(\mathbf{r}) = \nabla \times \mathbf{A}(\mathbf{r})$.

[18] We note that we are not creating a fully-mature dust devil of hundreds of meters in height but a minidust devil of

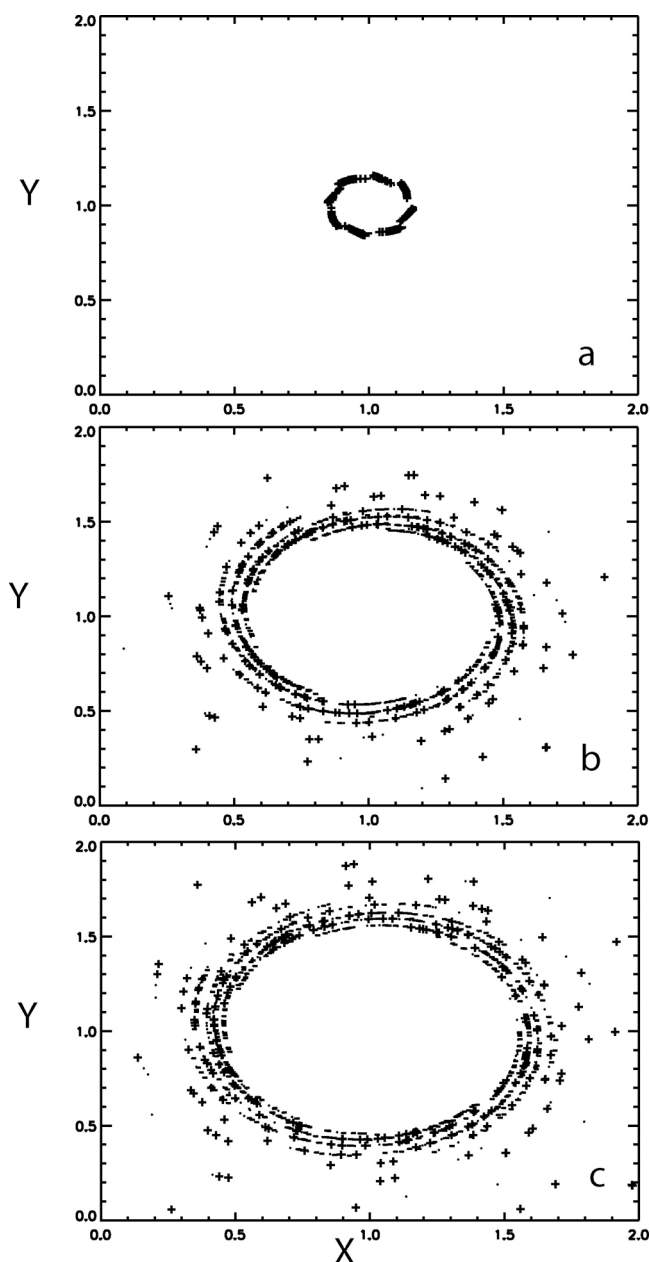


Figure 3. The grain X/Y positions after (a) 10 time steps, (b) 300 time steps, and (c) 499 time steps. Charged positive, negative, and neutral grains are indicated by pluses, minuses, and dots, respectively.

about ~ 0.5 m height and about 0.5 m in radius. Because of computational constraints, we instead are creating a small portion of a dust devil with entrained dust. However, as we discuss below, this small dusty cyclonic wind has the same characteristics as their larger counterparts. The computational constraints lie in modeling both microscopic charging processes at the micron-scale level but in a system on the scale size of a meter. While we simulate a smaller version of a dust devil, the physics can be scaled to a real system in order to understand the dynamics and associated E and B fields in a larger dust devil. A further discussion of the

model, scaling, and its application to a real system are included below.

3. Results

[19] Figure 3 shows the spatial distribution of grains in the x-y plane (i.e., grains viewed as if looking down from above the dust devil top). The grain charge polarization from contact electrification is also indicated by (–) negative, (+) positive, and (.) neutral symbols placed at each grain location. In this simulation, cyclostrophic winds are driving the grains and a vertical wind of 1 m/s is included. The simulation was initially seeded with 8 isolated sets of dust grains (i.e., 8 “clumps” of grains) equally-spaced on a circle about the dust devil center at a radius of 14 cm. Figures 3a, 3b, and 3c show the X/Y position of the grains after 10, 300 and 499 time steps, respectively. In Figure 3a, the grain clumps are evident, but also showing signs of smearing by the cyclostrophic winds. After the simulation has run for 300 time steps (Figure 3b), the lighter grains from each clump merge to form a quasi-continuum of small particles. These smaller particles are entrained in the winds and themselves move in near circular motion that mostly mimics the prevailing cyclostrophic wind pattern. However, intermediate and larger grains are more difficult to entrain and their inertia makes their movement less circular. Hence these particles tend to move outward toward the reflecting wall of the simulation. Near the end of the simulation (499 time steps, Figure 3c), some of the larger grains are approaching close to the wall, and the simulation is ceased at this time. The walls are reflecting and the particle remains in the simulation. However, these large insulator particles contain a large amount of collected charge (after numerous collisions) and their impulsive-like wall reflection gives rise to an abrupt change in current (since the velocity changes) and magnetic field. These boundary effects are thus avoided by the cessation of the simulation.

[20] Figure 4 shows the same grains, now viewed in a three-dimensional perspective in space. Note that the lighter grains remain in the upward spiral trajectory while heavier grains are not easily transported upward and are leaving the tighter spiraling group of particles. Such large grains in a real dust devil would be likely to exit the system, removing their positive charge from the moving dust column. The implications for this loss will be discussed below.

[21] The trajectories of the small and large grains become clear when one considered the $(v - v_g)^2$ factor in the wind force term of equation (6). For small, light grains, v_g goes from its initial value of 0 to near its maximum value of v in a few time steps. In contrast, many time steps are required for heavy grains to approach v . Entrainment is when $v_g \sim v$ and the particles are moving nearly force-free in the prevailing winds, and this process occurs much quicker for the smaller grains. However, even the smaller grains are not perfectly entrained with consistent radial movement over time (as evident in the increasing width of the dust devil eye in Figures 3a, 3b, and 3c).

[22] As mentioned above, the simulation presented here should not be considered that of an entire dust devil, but instead is a simulation of the evolution of a specific vertical portion or vertical slice of the dust devil that is about 0.3 m in vertical length, this starting from its particle injection to later

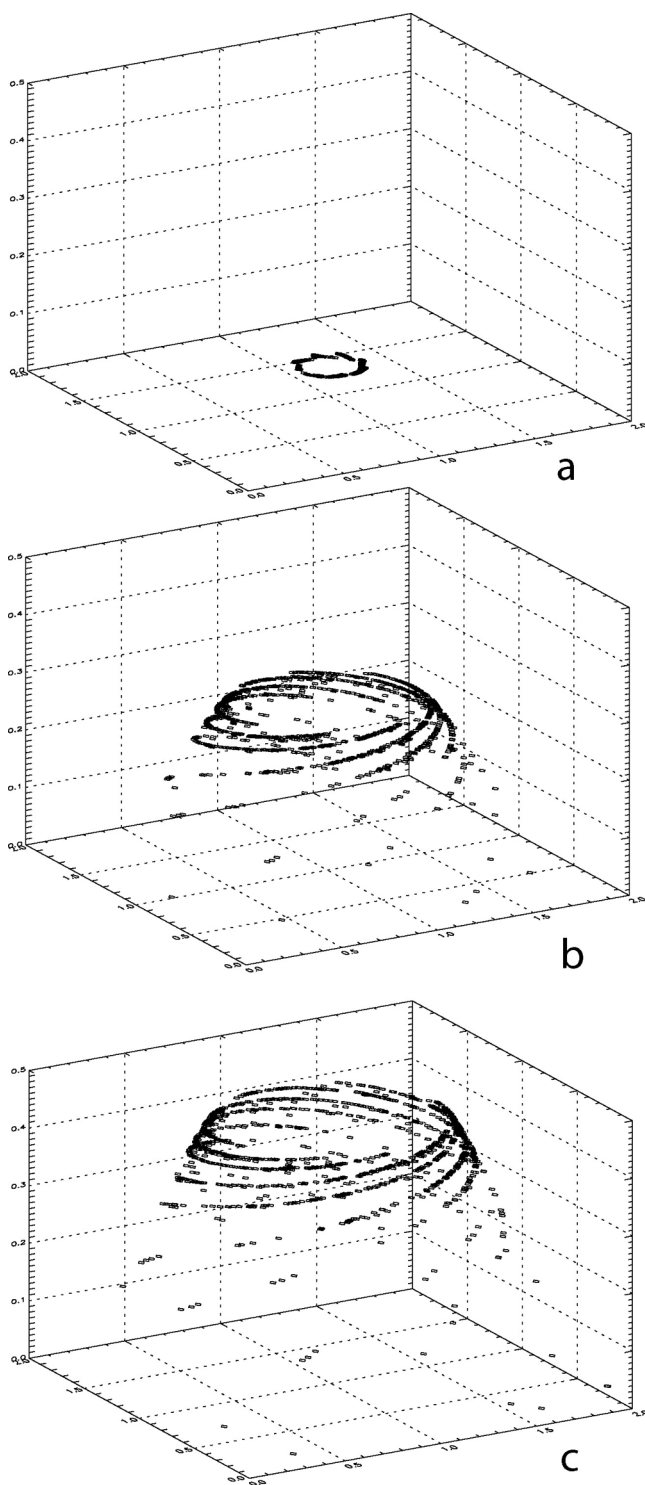


Figure 4. A three-dimensional perspective of the grains in the cyclostrophic/vertical winds at (a) 10 time steps, (b) 300 time steps, and (c) 499 time steps.

times. Figure 4 clearly illustrates this point. In essence, we are monitoring a segment of the dust devil created from the initial localized and discrete eight clumps at $t = 0$, these grains originating from a set of discrete locations along an assumed dust devils transverse path. In a real dust devil, continuous transverse movement of the structure would lift all clusters of

clumps along its path (making a continuous dust source) and these would fill in regions of space vertically, with earlier grain injections located at higher vertical heights and later grain injections as lower vertical heights. As such, there is a quasi-time stationary aspect to the evolution of the simulated grain dynamics which allows us to fill in the vertical portions of the dust devil using simulation results at different times. This scaling is not perfectly time stationary owing to collisions (which are random) and the nature of the entraining force which in early times varies as $(v - v_g)^2$. However, once entrained, the grain vertical movement should vary as t (see the derivation of equation (17) of Farrell *et al.* [2005]), with the vertical movement quasi-constant. Hence another way of looking at Figure 4 is to consider that we are examining a full dust devil at time t_0 , with Figure 4a showing those grains that have been injected at $t_0 - 10$ time steps, Figure 4b the grains at $t_0 - 300$ time steps, and Figure 4c the grains at $t_0 - 499$ time steps. The full dust devil would then be the superposition of these three figures, along with grains injected at all other time steps.

[23] In order to scale the simulated results from the eight discrete grain clumps to a real dust devil that is continuously extracting grains from the surface, we assume the real dust devil density has a density of about ~ 1 grain per cubic centimeter, thereby making the grain number density of the real-to-simulated dust devil, $n_r/n_{sim} \sim 10^3$. For a real system with 100 grains per cubic centimeter, the scaling goes as $n_r/n_{sim} \sim 10^5$.

[24] An obvious question to ask: Is such a scaling physically accurate? At early times (first 10 time steps), the grains undergo numerous collisions (like a real system in saltation). However, after this time, the grains are non-collisional with movement defined by the prevailing winds (see equation (6)). Scaling is most easily applied in this latter regime where the difference between simulated and real systems is simply a linear factor. Since our objective is to establish the E and B fields created in the dusty winds, the use of a representative but smaller grain population should only reduce the relative intensity of E and B, but not in any way limit the creation of the fields themselves.

[25] Figure 3 indicates that the smaller grains tend to become negatively charged upon collision. These smaller grains are also more entrained with the winds. In contrast, the heavy (+) grains tend to move more ballistically (not as circular) and appear to congregate along the outer edges of the dust devil. As an example, Figure 3c makes it evident that negative grains occupy the inner region near the dust devil core and positive grains have migrated to the dust devil outer region. In a real dust devil, some of these large positive grains would exit the system, but such particle loss is not modeled herein. The spatial separation of (+) grains to the outer region and (-) grains toward the inner region would in fact lead to a quasi-radial electrostatic field. The separation of (+) and (-) charge also leads to the development of an overall current in the dust devil and hence the development of a magnetic field. If both the (+) and (-) grains were moving at similar speeds, in a statistical sense, there would be no net current and no coherent B-field generation (possibly an incoherent B in association with local breaks in current cancellation).

[26] Figure 5 shows the final distribution of charge as a function of grain radius. We note that there are many more

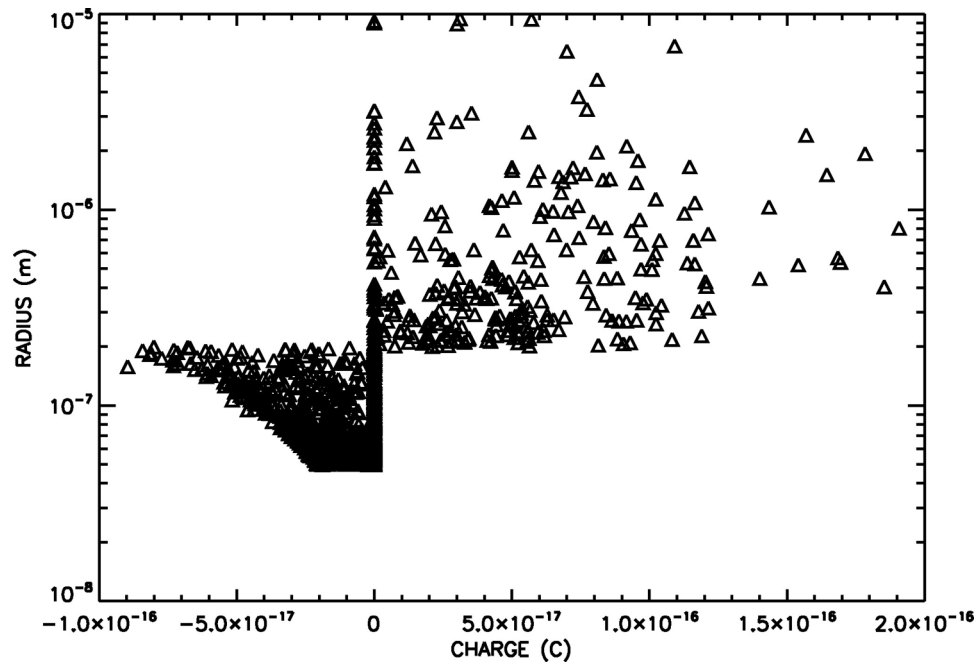


Figure 5. Distribution of grain charge as a function of grain radius. By design, particles with radii greater than 0.2 microns were assumed to be insulators and thus charge positive upon collision with smaller metallic negative-scavenging grains, as prescribed by the *Desch and Cuzzi* [2000] contact electrification algorithm. Note that charge is conserved in the system.

smaller (–) grains than large (+) grains, per our simulation design described previously. Some of the largest grains exceeding a micron have excess of 0.1 fC of charge as a result of numerous collisions with smaller grains. In our simulation, these grains tended to migrate toward the outer edge of the vortex, and may even be lost in a real dust devil.

[27] An obvious trend for smaller grains (the negatively charged grains, the distribution on the left-hand side of Figure 5) is the increasing grain capacity to hold charge as a

function of increasing radius. Specifically, as grain size increases, there is an increasing ability to hold more charge, as observed in the exponentially increasing charge limit as a function of radius defined by the edge of the distribution. This charge capacity is a direct result of using the *Desch and Cuzzi* [2000] formalism that includes both grain size and composition to derive the grain tribocharge exchange.

[28] Figure 6 shows the development of the magnetic field as a function of simulation run time for the case of insulator/metallic grain species with $\Delta\Phi = -1.6\text{V}$. As

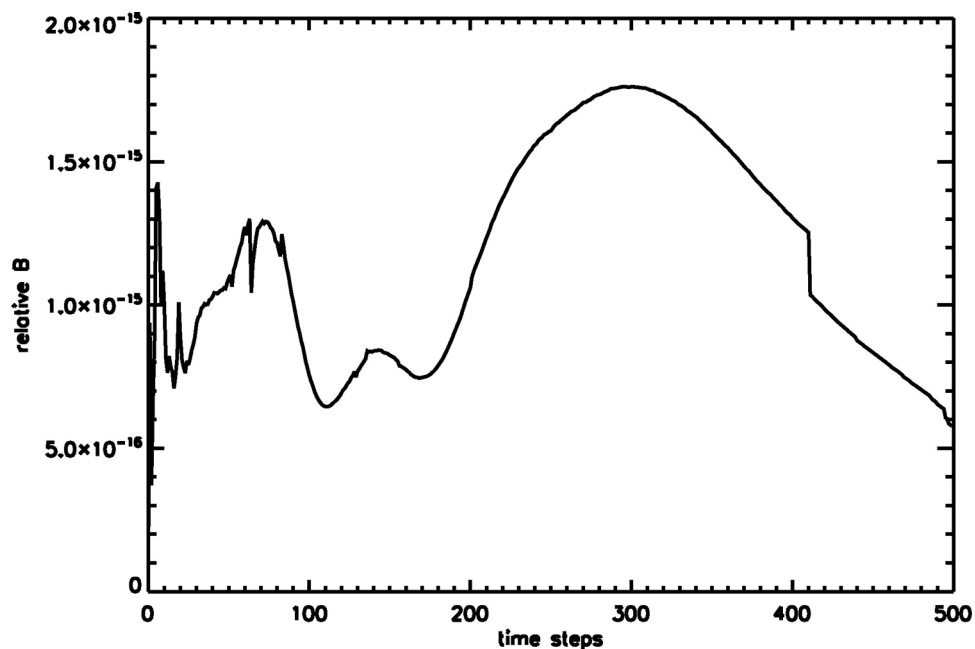


Figure 6. The magnetic field as a function of simulation time for $\Delta\Phi = -1.6\text{V}$.

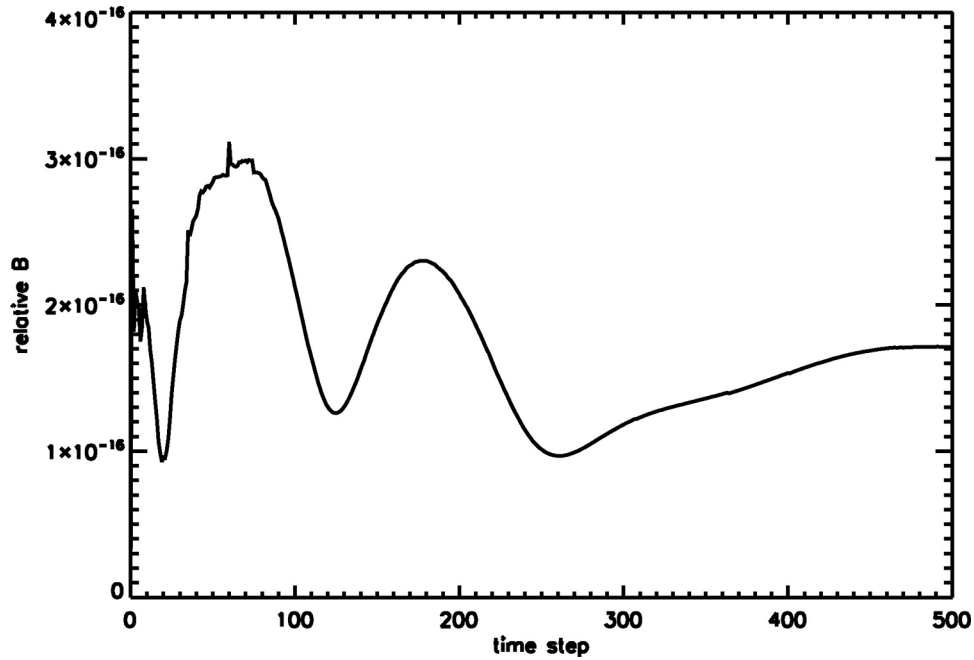


Figure 7. The magnetic field as a function of simulation time for $\Delta\Phi = -0.16$ V.

evident in the figure, there is a clear magnetic field generated from the circulating charges and this field appears to have an substantial AC component that would be detectable in a search coil antenna system like that described by *Houser et al.* [2003] and *Farrell et al.* [2004]. In theory, if the negative and positive grain distributions were of similar mass and radius distributions, then the net charge and current per unit volume would near zero and little/no B-field would be generated. However, as evident in Figure 5, grain charge is based upon radius (consistent with the Desch and Cuzzi model) and differing particle grain radii end up having differing trajectories (see Figure 3) resulting in a net current in the system. This net current yields the magnetic field.

[29] In order to approximately scale from the simulated relative B values in Figure 6 to real values for a large dust devil, we multiply the simulated B by $\mu_o/4\pi$ and $N_{\text{real}}/N_{\text{sim}}$ where $N_{\text{real,sim}}$ is the number of grains in the real and simulated dust devil, respectively. This scaling leads to values of B near 1 fT for dust devil densities near 3 grains/cc and $B \sim 100$ pT for densities near 100 grains per cc, which is at the lower end of detectability in modern day search coils. We note that our simulated grain population is in fact relatively small (limited to $<10 \mu\text{m}$ to allow particle reasonable particle movement in the simulated time). The capacity of a grain to hold charge varies directly with its radius and the addition of real grains of many tens of microns in size will add a significant current contribution as well. Also, we estimate that the tangential wind speed near the middle and end portion of the simulation to be relatively slow, only a few meters per second. In real dust devils this value might actually increase by a factor of 10, adding strength to the currents. In the simulation, the ratio of magnetic energy density to tangential kinetic energy density is about 10^{-16} . We note that the ratio of magnetic energy density to particle kinetic energy density in a real Arizona dust devil is also very weak [*Farrell et al.*, 2004], being nearly 10^{-11} . The larger real values relate to the presence of larger particles that hold

more charge and larger tangential wind speeds, both of which will increase the currents and the associated energy density. If both parameters increase by a factor of 10 in the simulations presented herein, the ratio of the energy densities between the real and simulated case become comparable.

[30] As evident in Figure 6, the magnetic field is not constant. It initially fluctuates quickly as the initially separate eight grain clumps begin their movement and merge into each other. As seen in Figure 3a, in the first ten time steps, the initially separate clumps begin to merge with currents from individual clumps vectorially adding to create a fast-fluctuating B. After about 40 time steps, the grains from individual clumps are merged and the fluctuation period becomes much longer, representing a slow-varying macroscopic current imbalance of the overall grain system. This current imbalance then creates the magnetic field.

[31] Figures 7 and 8 show the magnetic field for separate simulations run with the triboelectric potential difference, $\Delta\Phi$, reduced to $\Delta\Phi = -0.16$ V (Figure 7) and increased to $\Delta\Phi = -16$ V (Figure 8). All other parameters in these runs were held at the same values. It should be noted that the typical contact potential difference between insulators and conductors does not exceed 5V [see *Desch and Cuzzi*, 2000, Table 2]. However, an advantage of a simulation is the ability to conceive and test extreme situations in order to better understand the relationship of simulation variables. Such is the case here, where we find that the amount of current generated and the associated magnetic field varies in direct association with $\Delta\Phi$, with peak B fields being 3×10^{-16} , 1.8×10^{-15} and 3.5×10^{-14} in relative units for $\Delta\Phi = -0.16$, -1.6 and -16 Volts, respectively. The $\Delta\Phi = -16$ V in Figure 8 case is unrealistic, but provides a study for an imaginary extreme large contact potential case. We find for this case that there is an increase in charge exchange per grain, which in turn makes the overall current generation process more efficient, thereby increasing B. As illustrated in Figure 7, the opposite occurs in the case where

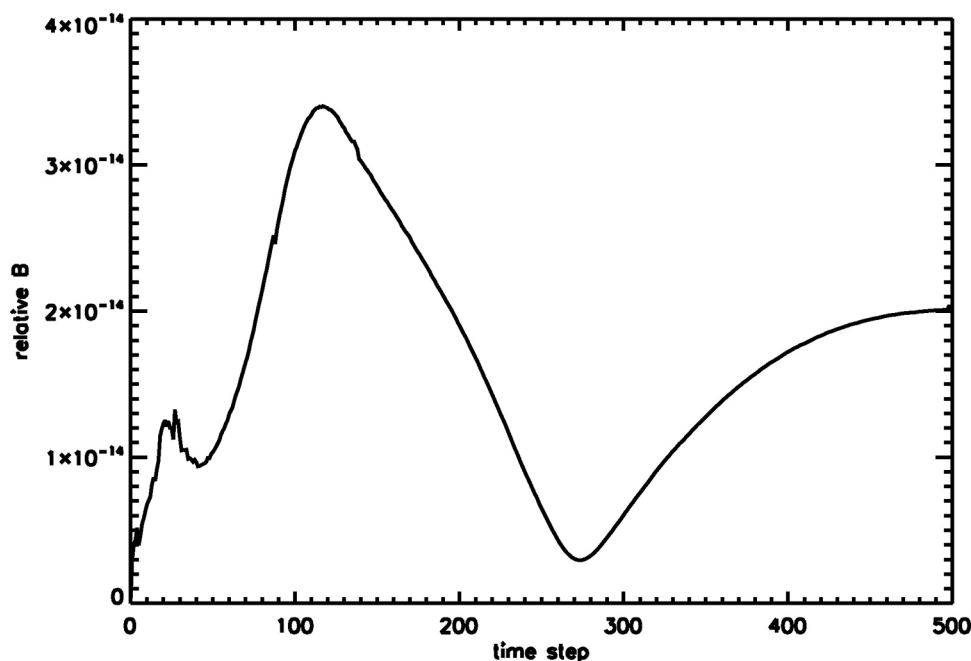


Figure 8. The magnetic field as a function of simulation time for $\Delta\Phi = -16.0$ V.

$\Delta\Phi = -0.16$ V. All cases show a B-field that is time-varying and thus detectable in a search coil.

4. Implications

[32] A curious aspects of Figures 6, 7 and 8 is the simulation of a relatively periodic variation in B, appearing as a quasi-monochromatic ULF signal that would be detectable in instruments like the search coil. This quasi-monochromatic variation is on timescales of 0.1–0.5 s and has distinct similarities to some cases observed in passing dust devils [Farrell *et al.*, 2004]. The timescale of the oscillation is approximately the timescale of rotation associated with the smallest grains. We suggest that the AC aspect of B is then associated with bunches of fast moving negative grains repeatedly passing bunches of slower larger positive grains. As these two groups of particles pass in proximity in the cyclostrophic winds, there is momentary local current cancellation and a minimum in B. When the two bunches are on opposite sides of a dust devil, their magnetic fields will add (vector addition) to create a local enhancement in B. The increasing period of the quasi-monochromatic fluctuation seen in all simulations results from two effects: First, the increasing speed of the positive grain bunch. This bunch is initially very slow and a faster negative grain bunch starting from the same location makes the circumference about the dust devil back to positive bunch in period t . However, as the positive grain bunch speed increases, it takes the (relatively) fast-circling smaller negative grain bunch progressively longer times to circumference the dust devil back to the positive bunch, $t' = t + \delta s/v_t$, where δs is the small azimuthal displacement for the positive grain bunch moving at tangential speed v_t . Second, the entire system is expanding radially outwards into weaker winds, slowing the spiral time for the negative grain bunches.

[33] The relative movement of small, negative and fast positive bunches in the azimuthally uniform wind field appear to be responsible for the weak AC B-fields observed in the simulation. However, if the wind field was not azimuthally uniform (an azimuthal inhomogeneity), it is easy to conceive of bunches formed locally along the edges of this wind velocity variation that would further increase the charge separation and current generation process.

[34] While we have focused on tangential currents to account for the B field, we also note the presence of vertical currents that can give rise to an overall vertical electric field. Figure 9 shows J_z in the simulation at time step = 300. Note

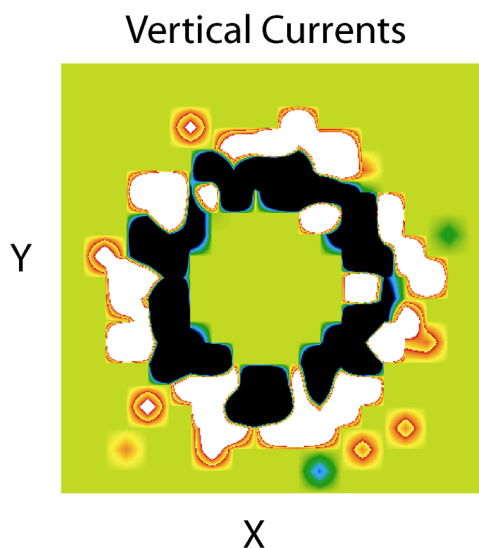


Figure 9. The vertical currents along the z-direction at $t = 300$ time steps. Note the development of negative currents (in black for values below -10^{-17} A/m²) near the eye wall while positive currents (white for values above $+10^{-17}$ A/m²) develop in the radially exterior regions.

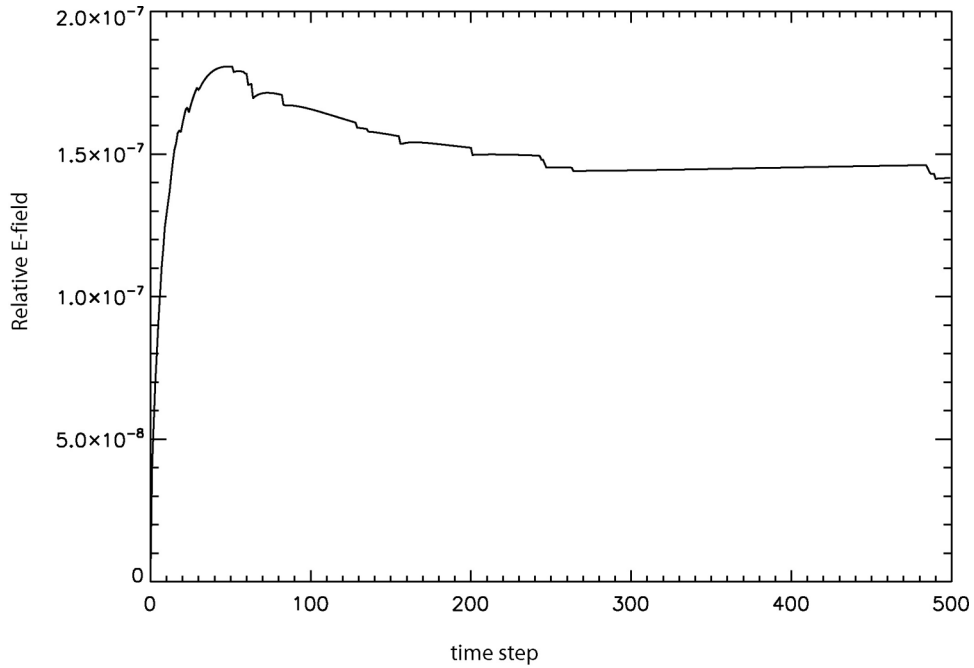


Figure 10. The development of the vertical electric field in the simulated set of grains, this due to the spatial separation from large positive and small negative grains.

that there are two regions of current: One negative current moving upward near the eye of the dust devil (black region) associated with the upward lifting of small negative grains and a second positive current located along the outer region of the system (white region) associated with the more massive positive grains. As demonstrated previously [Farrell *et al.*, 2003; Zhai *et al.*, 2006; Farrell *et al.*,

2005], these currents give rise to a vertical electric field. Specifically, in the vertical direction,

$$dE/dt = -(J_L + J_S + \sigma E)/\epsilon_0, \quad (7)$$

where J_L is the current from the large positive grains, J_S is the current from the small negative grains and σE is the

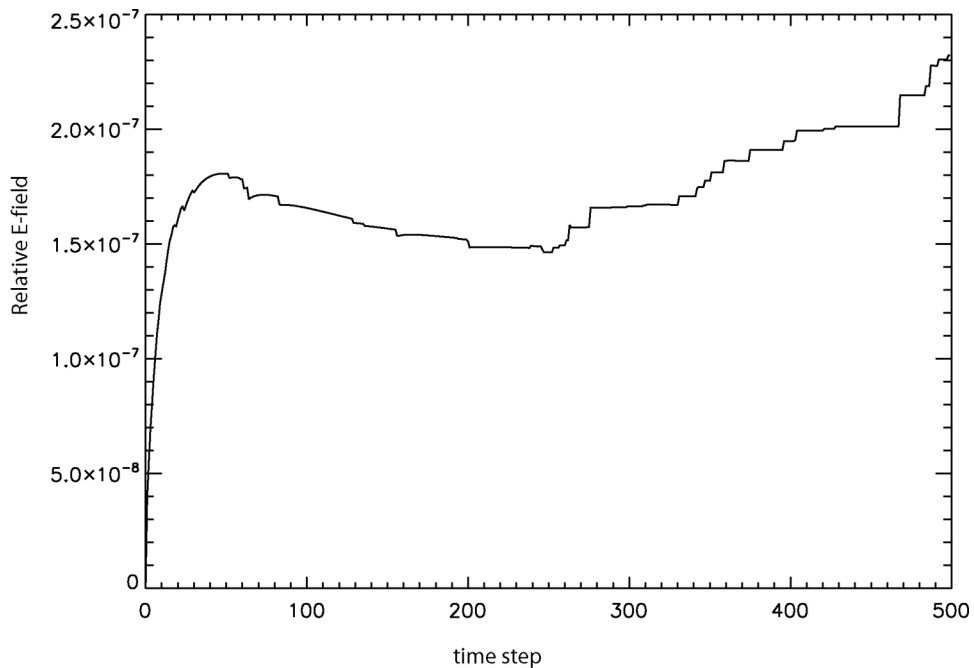


Figure 11. The development of the vertical electric field in the simulated set of grains, but now excluding the outermost grains (those assumed to have left the system).

atmospheric dissipation current. Figure 10 shows the relative vertical E field via integration of equation (7) assuming a low dissipation situation. Note that the temporal evolution of the E-field shows a distinct exponential rise like that modeled previously by *Melnik and Parrot* [1998], *Farrell et al.* [2003, 2005], and *Zhai et al.* [2006]. However, in our simulation, the E-field peaks and decreases slightly, reaching a quasi-steady value at about 200 time steps. The quasi-steady value is associated with internal current balance within the dust devil, with the exterior positive currents balancing the interior negative currents in the simulated case.

[35] We suspect that, in reality, the largest grains contributing to the exterior positive currents drop away from the moving dust devil and, in doing so, breaks the overall dust devil charge neutrality. There are two effects from positive grain loss: First, the small-grain negative currents will dominate and the E-field will again grow as a function of time (as opposed to remaining steady like in Figure 10). Second, with the loss of the positive grains, the dust devil develops a net monopole charge of negative value. To test this possibility, we recalculated the E-field using equation (7), but now with a J_z value derived from only those grains within in an areal area defined by $0.3 < x < 1.6$ and $0.3 < y < 1.6$. Grains outside this area (exclusively heavy neutral and positive grains; see Figure 3) are assumed to have been lost to the dust devil. Figure 11 shows the new E-field that begins to rise after 250 time steps with the dominance of the small-grain negative current. With the exclusion of exterior-located positive grains there will be the development of a net negative monopole to the dust devil. Thus, we expect that a real dust devil contains both a monopole and dipole term in its electrostatic expansion.

[36] Finally, Figures 3 and 4 show a segment of the dust devil that initially spirals around its center. However, over time, all grain trajectories migrate outward, creating an ever-increasing eye wall. The heavy grains with the greatest mass and inertia are the most difficult to entrain, while smaller grains congregate more centrally near the eye wall. This simulation using cyclostrophic balanced winds to drive the grains would suggest that the dust devil would have a pronounced broad-V funnel shape. However, in reality, many dust devils have a relatively tight column up to high altitudes. Real observations of a coherent column suggests that winds have to exceed cyclostrophic balance in order to maintain the grains at a constant radius about the center. These increased winds may be tangential (an increase in the cyclonic wind speed) that matches the added mass of the dust-entrained fluid element. In this case, a modification to equation (1) is required. Conversely, there may be an inward radial wind flow toward the dust devil center that would also act to maintain the dust devil column. A separate fluid equation independent of equation (1) would be required to describe this radial flow.

5. Conclusions

[37] We present a simulation of grain contact electrification in a wind pattern that mimics those in dust devils. This wind pattern contains transverse winds in cyclostrophic balance and a vertical wind component which together creates helical grain trajectories. We find that these helical

trajectories are different for large and small grains, with smaller grains tending to spiral close to the central eye region of the winds while heavier grains tending to move outward from the central region. Because of contact electrification, the smaller fast (metallic) grains near the central region are negatively charged and the larger slow (basaltic) grains in the outer region become positively charged.

[38] This spatial distribution of charged grains establishes a distinct current system involving the relative displacement of negative and positive charge in the dust devil. The transverse portion of this current is found to be responsible for a time-variable magnetic field while the vertical portion of this current is responsible for a large-scale vertical electrostatic E-field. Both fields have been observed previously in the vicinity of dust devils.

[39] From an electromagnetic perspective, we find that contact electrification of compositionally diverse grains in tandem with mass-stratifying winds are required properties of a dust devil to generate the observed fields reported previously. From a meteorological perspective, the horizontal winds in cyclostrophic balance cannot explain the columnar shape of the dust devil, and we suggest some additional wind flow either in the radial or tangential direction may be required to maintain a tight column to the convective feature.

[40] **Acknowledgment.** This work was funded by a 2002 NASA/Mars Fundamental Research Program (MFRP) award, which is heartily acknowledged.

References

- Beatty, D. W., et al. (2005), An analysis of the precursor measurements of Mars needed to reduce the risk of the first human mission to Mars, white paper, Mars Human Precursor Sci. Steer. Group, Jet Propul. Lab., Pasadena, Calif. (Available at http://images.spaceref.com/news/2005/MHP_SSG_06-02-051.pdf)
- Cahill, C. F., Y. Yee, T. E. Gill, A. Ruiz, S. P. Emmert, T. A. Cahill, F. Wilson, and E. Ellison (2005), Springtime dust aerosols at White Sands Missile Range, New Mexico, *Eos Trans. AGU.*, 86(52), Fall Meeting Suppl., Abstract P22B-02.
- Crozier, W. D. (1964), The electric field of a New Mexico dust devil, *J. Geophys. Res.*, 69, 5427.
- Delory, G. T., W. M. Farrell, B. Hillard, N. O. Rennó, P. Smith, J. R. Marshall, and A. Eatchel (2002), The electrical structure of terrestrial dust devils: Implications of multiple vertical measurements of the electric field, *Eos Trans. AGU.*, 83(47), Fall Meet. Suppl., abstract P51A-0335.
- Desch, S. J., and J. N. Cuzzi (2000), The generation of lightning in the solar nebula, *Icarus*, 143, 87.
- Eden, H. F., and B. Vonnegut (1973), Electrical breakdown cause by dust motion in low pressure atmospheres: Consideration for Mars, *Science*, 180, 962.
- Farrell, W. M., G. T. Delory, S. A. Cummer, and J. R. Marshall (2003), A simple electrodynamic model of a dust devil, *Geophys. Res. Lett.*, 30(20), 2050, doi:10.1029/2003GL017606.
- Farrell, W. M., et al. (2004), Electric and magnetic signatures of dust devils from the 2000–2001 MATADOR desert tests, *J. Geophys. Res.*, 109, E03004, doi:10.1029/2003JE002088.
- Farrell, W. M., N. Rennó, G. T. Delory, S. A. Cummer, and J. R. Marshall (2005), Integration of electrostatic and fluid dynamics within a dust devil, *J. Geophys. Res.*, 111, E01006, doi:10.1029/2005JE002527.
- Freier, G. D. (1960), The electric field of a large dust devil, *J. Geophys. Res.*, 65, 3504.
- Greeley, R., et al. (1992), Martian aeolian process, sediments and features, in *Mars*, edited by H. H. Kieffer et al., p. 730, Univ. of Ariz. Press, Tucson.
- Greeley, R., M. R. Balme, J. D. Iversen, S. Metzger, R. Mickelson, J. Phoremman, and B. White (2003), Martian dust devils: Laboratory simulations of particle threshold, *J. Geophys. Res.*, 108(E5), 5041, doi:10.1029/2002JE001987.

- Houser, J. G., W. M. Farrell, and S. M. Metzger (2003), ULF and ELF magnetic activity from a terrestrial dust devil, *Geophys. Res. Lett.*, *30*(1), 1027, doi:10.1029/2001GL014144.
- Jackson, T. L., and W. M. Farrell (2006), Electrostatic fields in dust devils: An analog to Mars, *IEEE Trans. Geosci. Remote Sens.*, *44*, 2942.
- Melnik, O., and M. Parrot (1998), Electrostatic discharge in Martian dust storms, *J. Geophys. Res.*, *103*, 29107.
- Mills, A. A. (1977), Dust cloud and frictional generation of glow discharges on Mars, *Nature*, *268*, 614.
- Rennó, N. O., and A. P. Ingersoll (1996), Natural convection as a heat engine: A theory for CAPE, *J. Atmos. Sci.*, *53*, 572.
- Rennó, N. O., M. L. Burkett, and M. P. Larkin (1998), A simple thermodynamical theory for dust devils, *J. Atmos. Sci.*, *55*, 3244.
- Ryan, J. A., and R. D. Lucich (1983), Possible dust devils, vortices on Mars, *J. Geophys. Res.*, *88*, 11,005.
- Zhai, Y., S. A. Cummer, and W. M. Farrell (2006), Quasi-electrostatic field simulations of Martian dust storms, *J. Geophys. Res.*, *111*, E06016, doi:10.1029/2005JE002618.

S. A. Cummer, Department of Electrical and Computer Engineering, Duke University, Box 90291, Durham, NC 27708, USA.

G. T. Delory, Space Sciences Laboratory, University of California, Berkeley, Berkeley, CA 94720, USA.

M. D. Desch and W. M. Farrell, NASA/Goddard Space Flight Center, Code 695, Greenbelt, MD 20771, USA. (william.farrell@gsfc.nasa.gov)

J. R. Marshall, SETI Institute, 515 North Whisman Road, Mountain View, CA 94043, USA.